Polymer Electrochromism Driven by Metabolic Activity Facilitates Rapid and Facile Bacterial Detection and Susceptibility Evaluation

Jiayingzi Wu, Yifan Zhu, Liyan You, Pu-Ting Dong, Jianguo Mei,* and Ji-Xin Cheng*

The electrochromism of a water-soluble naturally oxidized electrochromic polymer, ox-PPE, is harnessed for rapid and facile bacterial detection, discrimination, and susceptibility testing. The ox-PPE solution shows distinct colorimetric and spectroscopic changes within 30 min when mixed with live bacteria. For the underlying mechanism, it is found that ox-PPE responds to the reducing species (e.g., cysteine and glutathione) released by metabolically active bacteria. This reduction reaction is ubiquitous among various bacterial strains, with a noticeable difference that enables discrimination of Gram-negative and Gram-positive bacterial strains. Combining ox-PPE with antibiotics, methicillin-susceptible and methicillin-resistant *Staphylococcus aureus* can be differentiated within 2.5 h. Proof-of-concept demonstration of ox-PPE for antimicrobial susceptibility testing is carried out by incubating *Escherichia coli* with various antibiotics. The obtained minimum inhibition concentrations are consistent with the conventional culture-based methods, but with the procedure time significantly shortened to 3 h.

1. Introduction

Electrochromism is generally defined as a reversible color change of an electroactive material in accompaniment with a chemical or electrochemical doping process, which can be realized upon addition of chemical dopants (reducing/oxidizing agents) or application of an appropriate voltage.[1] Being able

Dr. J. Wu, Dr. L. You, Prof. J. Mei
Department of Chemistry
Purdue University
West Lafayette, IN 47907, USA
E-mail: jgmei@purdue.edu
Y. Zhu, Dr. P.-T. Dong, Prof. J.-X. Cheng
Department of Chemistry
Department of Electrical and Computer Engineering
Boston University
Boston, MA 02215, USA
E-mail: jxcheng@bu.edu
Prof. J.-X. Cheng
Department of Physics
Department of Biomedical Engineering
Boston University
Boston, MA 02215, USA

The ORCID identification number(s) for the author(s) of this article can be found under https://doi.org/10.1002/adfm.202005192.

to change the color upon applied voltages, electrochromic devices have shown wide applications in self-dimming mirrors, smart windows, information displays, data-storage devices, sunglasses, and fabric electrochromics.[2] Among the electrochromic materials, conjugated polymers have received significant attentions because of their rapid response, high optical contrast, processability, and easy tuning of color with alternations in the structures.[3] While polymer-based electrochromic devices are maturing toward customer products, investigation of polymer electrochromism for biological applications are still in infancy.[4] Due to their unique sensitivity to protons, electrons and chemicals, electrochromic polymers are attractive candidates for developing biosensors.[5] It is appealing to measure biological events by absorption spectroscopy with a simple instrument or directly by visible color change with naked eyes.[6]

Bacteria are associated with broad-spectrum metabolic activities at molecular levels, which can be harnessed for electrochromic detection. For example, bacteria metabolize glucose and release mixed acids like succinate, acetate, malate, etc., as byproducts. As shown in the previous study, those acidic metabolites could trigger the transition of electrochromic polymer polyaniline from its emeraldine base form to its emeraldine salt form, leading to a visible color change from blue to green.[7] However, the low aqueous solubility and the instability of pristine polyaniline in an aqueous solution hinders its applications for in situ sensing in the solution state. Besides the pH changes, redox components also play important roles in bacterial metabolism. Trans-plasma membrane electron transport is a widespread property of respiring bacteria, linking intracellular metabolism with extracellular electron acceptors.[8] Thus, electrochromic dyes and metal oxides that are capable to accept electrons have been explored as potent redox probes of bacteria. Previously, tungsten trioxide, one of the most broadly used inorganic electrochromic materials, was utilized for bacterial detection via extracellular electron transfer.[9] Nevertheless, its applications are mainly limited to the exoelectrogenic bacteria thriving in anaerobic conditions and the synthesis of tungsten trioxide nanoclusters also remains complex. Meanwhile, several redox-active dyes have also been reported as viability indicators, a majority of which are directly reduced by plasma

**ADVANCED
SCIENCE NEWS**
www.advancedsciencenews.com

**ADVANCED
FUNCTIONAL
MATERIALS**
www.afm-journal.de

or/and membrane dehydrogenase enzymes to achieve the detection.[8c,10] However, they mostly measure bacterial viability rather than activity,[11] and some of them are toxic to cells, giving rise to an underestimation of viable bacteria.[12] Last but not the least, bacteria also excrete reducing agents (e.g., cysteine, glutathione (GSH)) and thiol proteins) into the medium, as a result of metabolic activity, antioxidant defense and redox homeostasis.[13] Those extracellular metabolites provide another possible mechanism for reduction of electrochromic electron acceptors, which has not been fully investigated yet.

Here, we report an aqueous soluble electrochromic poly(3,4-propylenedioxythiophen-alt-3,4-ethylenedioxythiophene) copolymer (PPE) as a novel sensor of metabolically active bacteria. PPE was conventionally used as a material to control the color of a electrochromic device.[14] Due to its low oxidation potential, PPE can be naturally doped by ambient oxygen to form an oxidized state (ox-PPE). We find that the ox-PPE can be dedoped (reduced) by metabolically active bacteria. The reduction process is associated with visual color changes of ox-PPE, as well as distinct absorption spectroscopic changes measured with a 96-well microplate reader in a high-throughput fashion. The primary mechanism of the reduction could be attributed to extracellular metabolites because addition of cell-free supernatants triggered the reduction activity of ox-PPE and no binding of ox-PPE on bacterial membranes was observed. Particularly, the reduction shows high sensitivity and specificity to cysteine and GSH. The electrochromism of ox-PPE enables rapid and facile bacterial detection, discrimination of Gram-positive and Gram-negative bacteria, as well as antimicrobial susceptibility testing.

2. Results and Discussion

2.1. Electrochromic Properties of PPE/ox-PPE

The color of PPE can be tuned through electrochemical reactions (**Figure 1**a). As shown in Figure 1b, upon electrochemical oxidation, a PPE film switched from a blue colored state in the visible region (−600 mV vs Ag/AgCl) to a bleached state in the near-infrared region (310 mV vs Ag/AgCl). Similar to other ProDOT$_x$EDOT$_y$ copolymers, the absorption peak at ≈600 nm is corresponding to the neutral PPE, and the absorption >1500 nm is corresponding to the bipolaron band as a result of complete oxidation.[14] In addition, partial oxidation leads to the formation of polarons, which causes the absorption ≈1000 nm. Importantly, due to its low oxidation potential,[14a] PPE in the aqueous solution (pH = 7.4) can be directly oxidized by ambient oxygen and mostly converted into bipolarons (Figure 1c). The naturally oxidized PPE (ox-PPE) possesses high stability in aqueous solutions (data not shown here) and the avoidance of using any toxic oxidant diminishes the cytotoxicity to mammalian cells. Additionally, the adequate aqueous solubility of ox-PPE offers close contact with the analytes in the solution. Taken together, these attractive features of electrochromic ox-PPE make it an excellent candidate for biosensing and inspired us to explore its response to bacteria.

2.2. Colorimetric Response of ox-PPE to Bacteria

For our initial test, we used *Escherichia coli* (*E. coli*) ATCC 25922 as a model analyte, cultured in a minimal salt (M9) medium
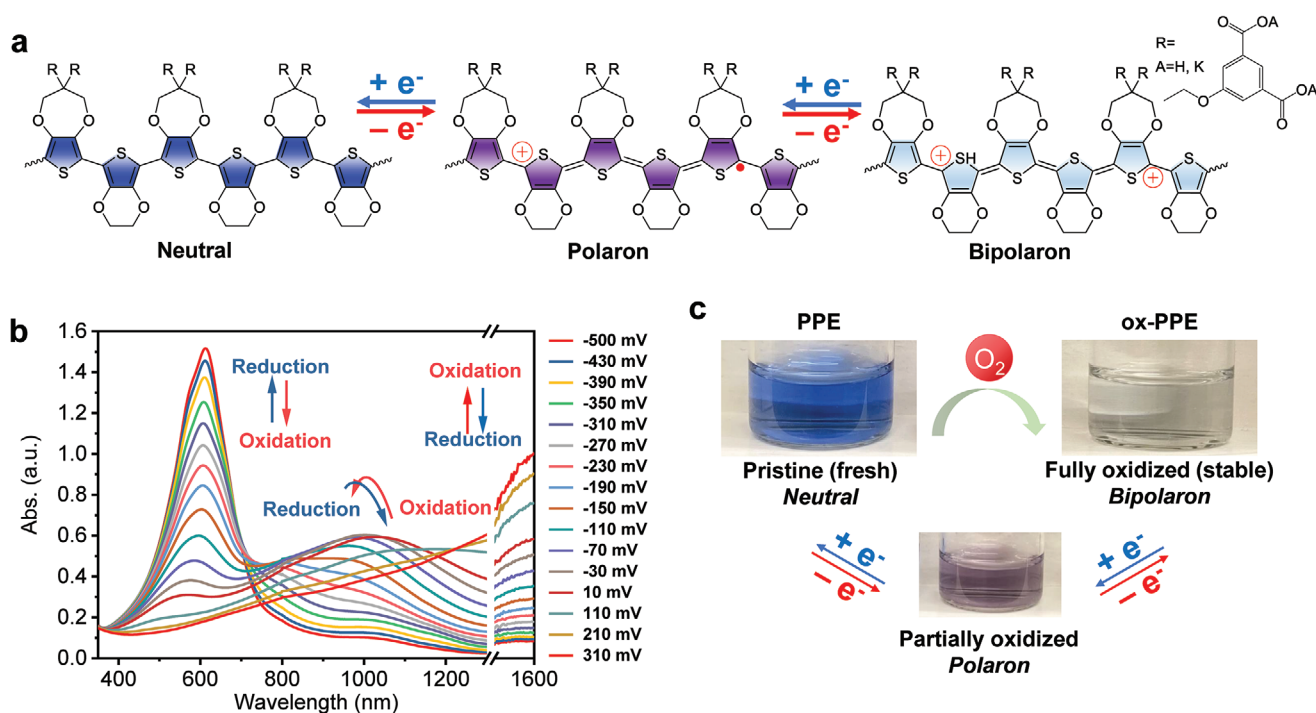

Figure 1. Electrochromic properties of PPE/ox-PPE. a) Schematic illustration of PPE in different oxidation states. b) Spectroelectrochemistry of PPE in response to electrochemical oxidation upon applied voltages. c) Photographic images of PPE aqueous solutions in neutral state (with N$_2$H$_4$ reducing agent), or in polaron/bipolaron (ox-PPE) state after ambient oxygen oxidation.
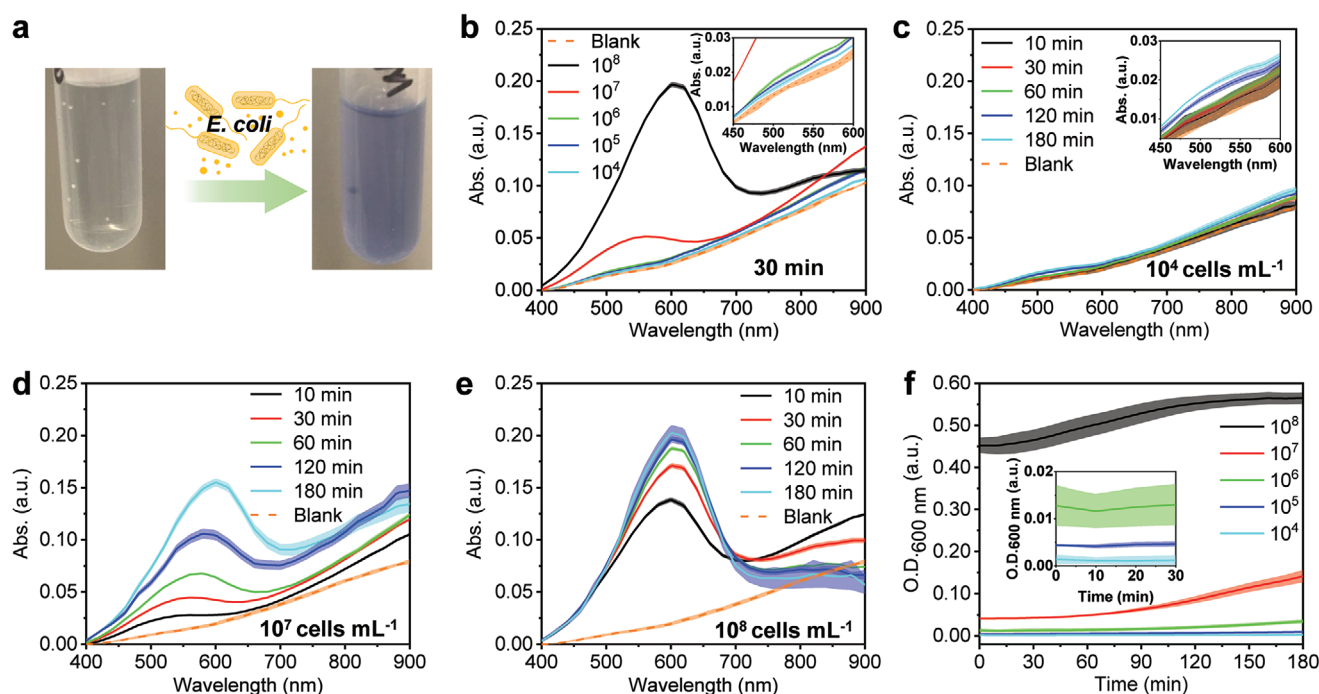
Figure 2. Colorimetric response of ox-PPE to *E. coli*. a) Photographic images of ox-PPE solution without or with *E. coli*. b) Responses of ox-PPE to different concentrations of *E. coli*. Absorption spectra were recorded after 30 min reaction. Kinetic responses of ox-PPE upon addition of c) 10^4 cells mL^{-1}, d) 10^7 cells mL^{-1}, and e) 10^8 cells mL^{-1} *E. coli*. f) Growth of *E. coli* monitored by the optical density (O.D.) at 600 nm. Error bars represent standard deviation of triplicate measurements.

containing 0.4% glucose. A significant color change of ox-PPE was found after incubation with *E. coli* (**Figure 2**a), which means ox-PPE could be potentially used as a microbial probe. We then performed more detailed investigations, in order to find the optimal detection conditions as well as the detection limit. The absorption spectra of ox-PPE were recorded with a 96-well microplate reader, which brings the benefit of high-throughput detection and large-scale antibiotic screening.[15] It is also worth mentioning that our method does not require washing steps, which simplifies the experimental procedure, shortens the procedure time, and avoids the potential loss of bacteria.[15b] First, we investigated the optimal concentration of ox-PPE for bacterial detection. Among the three tested concentrations of ox-PPE (12.5, 25, and 50 µg mL^{-1}), the reduction is more obvious with a lower concentration of ox-PPE (Figure S1, Supporting Information). This could be explained by the reaction equilibrium that the relatively less ox-PPE would drive the reaction more toward the right-side. However, limited by the sensitivity of the instrument, lower concentration associates with lower signal-to-noise ratio and larger signal fluctuations. Thus, 25 µg mL^{-1} was chosen for the following studies, as a complementary between the percentage of reduction and the signal-to-noise ratio. Next, we examined the response of ox-PPE to the varied concentrations of *E. coli* after a short incubation time (30 min). 10^7 and 10^8 cells mL^{-1} bacteria were discerned by the visible color change after 30 min, validating the potential of ox-PPE as a colorimetric sensor (Figure S2, Supporting Information). The detection sensitivity was further improved with absorption spectroscopy measurements. As shown in Figure 2b, we could reproducibly differentiate bacterial levels as low as

10^4 cells mL^{-1} from the recorded absorption spectra. The detection limit of 10^4 cells mL^{-1} meets the requirement of clinical applications,[16] and the 30 min reaction time is much shorter than the traditional culture-based methods.[17]

Then, we studied the culture time-dependency with different concentrations of *E. coli*. For bacteria with a 10^4 cells mL^{-1} initial concentration, slight increase occurred from 10 to 180 min (Figure 2c). Differently, the spectra changed significantly and continuously for bacteria with a 10^7 cells mL^{-1} initial concentration within 180 min (Figure 2d). For a 10^8 cells mL^{-1} initial concentration, significant increase of absorption at ≈600 nm was found within 60 min, but no further increase was noticed after 120 min (Figure 2e). To understand the observed time-dependency, we monitored the growth of bacteria via an optical density measurement. Figure 2f shows that bacteria with a 10^4 cells mL^{-1} initial concentration had negligible growth within 180 min as in the lag phase, while bacteria with a 10^7 cells mL^{-1} initial concentration were growing more rapidly as in the log phase. The growth rate of bacteria with a 10^8 cells mL^{-1} initial concentration reached the plateau after 120 min, entering the stationary phase. Therefore, the obtained time-dependency and bacterial concentration-dependency could be attributed to two factors: bacterial population and metabolic activity.

2.3. Mechanism of the Bacteria-Driven Electrochromism

To figure out whether the reduction of ox-PPE is mediated by the metabolic activity of bacteria, we carried out glucose-dependent and temperature-dependent measurements. We chose glucose
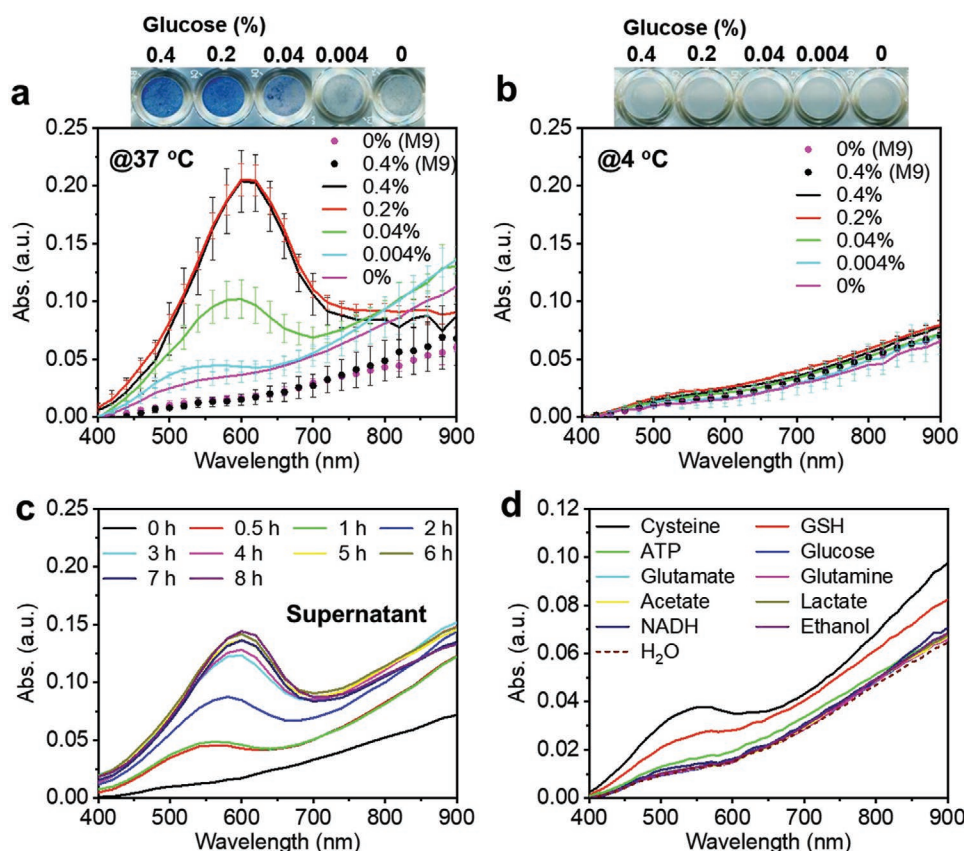
**ADVANCED
SCIENCE NEWS**
www.advancedsciencenews.com

**ADVANCED
FUNCTIONAL
MATERIALS**
www.afm-journal.de

Figure 3. Colorimetric responses of ox-PPE to *E. coli* (10^8 cells mL^{-1} in M9 medium) cultured with different concentrations of glucose, supernatant, and various reducing molecules. a,b) Absorption spectra at 37 and 4 °C, respectively, recorded after 2 h reaction. At the tops, photographic images of microplate wells showing the color change upon variation of the glucose concentrations at 37 and 4 °C, respectively. c) Response of ox-PPE to supernatants derived from *E. coli* suspensions (10^8 cells mL^{-1} in M9 medium containing 0.4% glucose) collected at different incubation times. d) Response of ox-PPE to different reducing agents (200×10^{-6} M). Absorption spectra were recorded after 30 min reaction. GSH: glutathione; ATP: adenosine 5'-triphosphate; NADH: diphosphopyridine nucleotide. Error bars represent standard deviation of triplicate measurements.

because it is an essential carbon source to maintain the bacterial metabolism.[18] A strong correlation between the reduction level of ox-PPE and the concentration of glucose in the M9 medium (**Figure 3**a) indicates that the reaction was driven by glucose-dependent metabolic processes. In addition, when the metabolic activity was suppressed at a low temperature (4 °C), the reduction of ox-PPE was also diminished (Figure 3b). Taken together, we show that the reduction of ox-PPE is mediated by metabolic active bacteria. Therefore, ox-PPE is capable to differentiate live bacteria from dead bacteria and can be potentially used to detect slow-growing bacteria.[19]

We then moved forward to study what metabolic products cause the reduction of ox-PPE. Previously, we have demonstrated that the broad-absorbing conjugated polymer could be imaged with a transient-absorption (TA) microscope.[20] Here, ox-PPE was also found to be a good TA contrast agent (Figure S3a, Supporting Information). To check whether ox-PPE bound to bacteria, we performed TA imaging of *E. coli* incubated with ox-PPE for 2 h and then washed with PBS for three times. Negligible TA signals of ox-PPE were found on bacterial membrane or inside bacteria (Figure S3b,c, Supporting Information), indicating that ox-PPE did not bind to or enter the bacteria. We then collected a series of cell-free

supernatants from *E. coli* (O.D.$_{600}$ = 0.5) incubated for different periods of time (1–8 h) in M9 medium containing 0.4% glucose. As expected, the supernatants caused the reduction of ox-PPE, with a positive correlation between the culture time and the reaction level (Figure 3c) similar to that in Figure 2d. A group of reducing molecules that commonly exist in a bacterial culture medium were then tested separately. Figure 3d reveals that cysteine and GSH induced obvious reduction of ox-PPE, while other reducing molecules showed minor interactions with ox-PPE. As shown in Figure S4 in the Supporting Information, ox-PPE could detect cysteine with the concentration as low as <4.9×10^{-6} M. It has been known that bacteria develop functional systems for cysteine excretion, because a high intracellular concentration of cysteine may be toxic to cells.[13b,c] Extracellular concentration of cysteine was reported as 40×10^{-6}–250×10^{-6} M, depending on the strains.[21] Meanwhile, extracellular GSH plays an important role in antioxidant defense and redox homeostasis.[13a] The concentration of extracellular GSH was estimated as 2.7×10^{-6} M for *E.coli* K-12 at log-growth and 24×10^{-6} M for *Salmonella typhimurium* TA1534 at early stationary phase.[22] Collectively, our data show that reduction of ox-PPE is likely to be dominated by cysteine- and GSH-metabolism.

2.4. Detection and Differentiation of Gram-Negative and Gram-Positive Bacteria

With the underlying mechanism studied, we further explored the practical applications of ox-PPE reduction. We first validated the generality of the reduction reaction with three Gram-positive strains (*Staphylococcus aureus* (*S. aureus*) ATCC 6538, Methicillin-resistant *S. aureus* (MRSA) USA 300 and *E. faecalis* NR-31970) and five Gram-negative strains (*E. enterica* ATCC 700720, *E. coli* ATCC 25922, *E. coli* BW 25113, *Enterobacter cloacae* ATCC BAA-1143, and *Acinetobacter baumannii* ATCC BAA-1605). For all the eight strains (O.D.$_{600}$ = 0.5), substantial spectroscopic changes of ox-PPE were observed after 30 min reaction in Mueller Hinton Broth (MHB) medium (**Figure 4**a). Intriguingly, a spectroscopic difference in the 700–900 nm window was noticed between Gram-negative and Gram-positive strains. To answer whether such difference is sufficient to differentiate the two groups, principal component analysis (PCA), which converts a group of variables into some linearly uncorrelated variables using orthogonal transformation,[23] was performed on the absorption spectra of ox-PPE for individual bacterial strain (from three replicated measurements). The PCA result shown in Figure 4b indicates that Gram-negative and Gram-positive bacteria can be discriminated by ox-PPE within 30 min.

In order to make a more insightful analysis of the interactions between ox-PPE and bacteria, quantification of the reduction level of ox-PPE is demanded. Yet, the reduction level is not directly related to absorption intensity at any single wavelength. Hence, we decomposed the absorption spectra of PPE in Figure 1b into neutral, polaron, and bipolaron states (Figure 4c) by potentiometric UV–vis titration and corresponding chemical equilibrium fitting.[24] Then, the decomposed spectra were used as reference spectra for non-negative linear least square fitting of an unknown spectrum to extract the relative concentrations of polymers in neutral, polaron, and bipolaron states, represented by [N], [P], and [BP], respectively (Figure 4d).[24] Subsequently, the reduction level can be quantitated by the fraction of
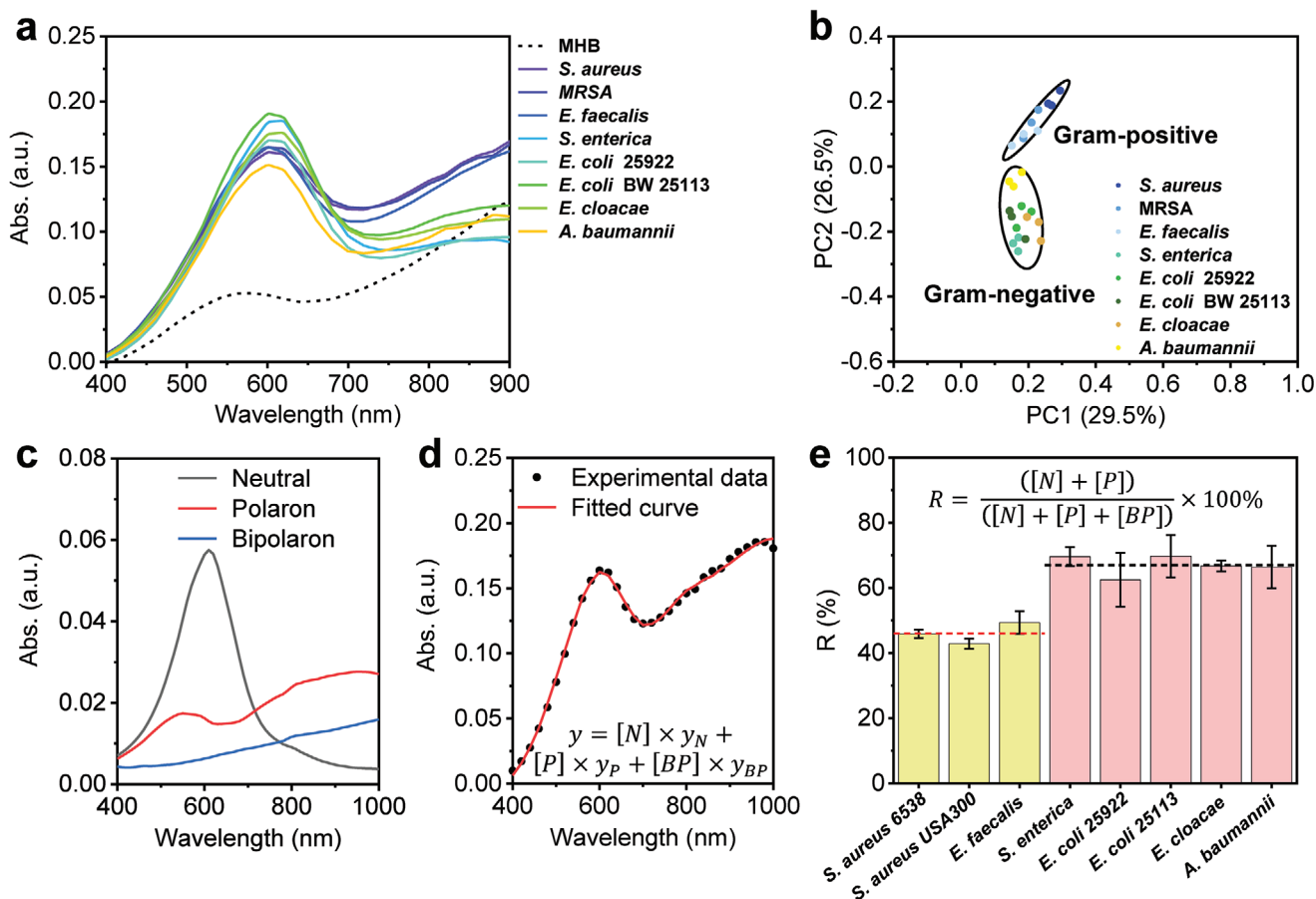

Figure 4. Differentiation of Gram-positive and Gram-negative strains by ox-PPE. a) Absorption spectra of ox-PPE incubated with different bacterial strains (10^8 cells mL^{-1} in MHB medium). Absorption spectra were recorded after 30 min reaction. b) PCA analysis of the data in (a) for discrimination between Gram-negative and Gram-positive strains. 90% confidence ellipses for Gram-negative and Gram-positive strains are depicted. c) Absorption spectra of neutral, polaron, and bipolaron states derived from potentiometric UV–vis titration. d) The experimental data curve and the fitted curve of the absorption of ox-PPE in *S. aureus* 6538 as an example for linear least squared fitting. γ_N, γ_P, and γ_{NP} are the absorption spectra of neutral, polaron, and bipolaron states in (c). [N], [P], and [NP] represent concentrations of neutral, polaron, and bipolaron states. $R^2 > 0.99$. e) The reduction levels of ox-PPE for different bacterial strains. Error bars represent standard deviation of triplicate measurements.

**ADVANCED
SCIENCE NEWS**

www.advancedsciencenews.com

**ADVANCED
FUNCTIONAL
MATERIALS**

www.afm-journal.de

molecules (R) that is converted from bipolaron to polaron and neutral state

$$R = \frac{([N]+[P])}{([N]+[P]+[BP])} \times 100\% \quad (1)$$

The calculated reduction levels of ox-PPE with different bacterial strains are shown in Figure 4e, revealing that ox-PPE was more reduced by Gram-negative strains than by Gram-positive strains. One possible reason for such difference is that most Gram-positive bacteria do not produce GSH, while other alternative (protein) thiols have less negative redox potential than GSH.[25]

2.5. Rapid Antibiotic Susceptibility Testing

Antibiotic attack causes a very fast and massive change in bacterial transcription profile, and thus leads to decrease in protein synthesis and in metabolic activity.[26] Such metabolism shock associated with the immediate cellular response can be harnessed to probe the bacterial susceptibility to antibiotics.[18b] Therefore, we tested the feasibility of using ox-PPE to differentiate between *S. aureus* strains with clinically relevant resistance and susceptibility in their responses to antibiotics. Susceptible *S. aureus* ATCC 6538 and MRSA USA300 were grown to the log phase and then diluted to a concentration of ≈5 × 10^7 cells mL^{-1} (O.D.$_{600}$ = 0.25) in MHB medium. The bacteria were treated

with varied concentrations of methicillin (0–80 μg mL^{-1}) for 2 h; ox-PPE was then added into the suspensions for another 30 min incubation. The suspensions were subjected to absorption spectroscopic measurement, and the antimicrobial susceptibility was characterized by the relative reduction degree ($R - R_b$)/($R_0 - R_b$), of experimental groups ($R - R_b$) with respect to the control group ($R_0 - R_b$) in which no antibiotic was added.[15b] R_b is the reduction level of ox-PPE alone in MHB and R_0 is the reduction level of the control group. **Figure 5**a shows that metabolic activity of susceptible *S. aureus* was significantly inhibited after being treated with 1.25 μg mL^{-1} methicillin. On the contrary, no significant change was observed in MRSA treated with methicillin at concentrations up to 80 μg mL^{-1} (Figure 5b). The critical points in the metabolic activity tests where the reduction levels drop significantly are consistent with the minimum inhibition concentration (MIC) values determined by the conventional culture-based method (18 h incubation) (Figure 5c,d). Hence, the MRSA was clearly distinguished from susceptible *S. aureus* by using ox-PPE within a short time (2.5 h).

We then explored the potential of ox-PPE to quantitate the effectiveness of different antibiotics including ciprofloxacin (CIP), ofloxacin (OFL), polymyxin B (PMB), tetracycline (TET), erythromycin (ERY), oxacillin (OXA). *E. coli* ATCC 25922 was cultured to the log phase in tryptic soy medium, and then centrifuged and resuspended in glucose-containing M9 medium at a concentration of ≈5 × 10^7 cells mL^{-1} (O.D.$_{600}$ = 0.25). The bacteria were treated with different antibiotics at varied concentrations (0–80 μg mL^{-1}) for 2 h. Subsequently, ox-PPE was added
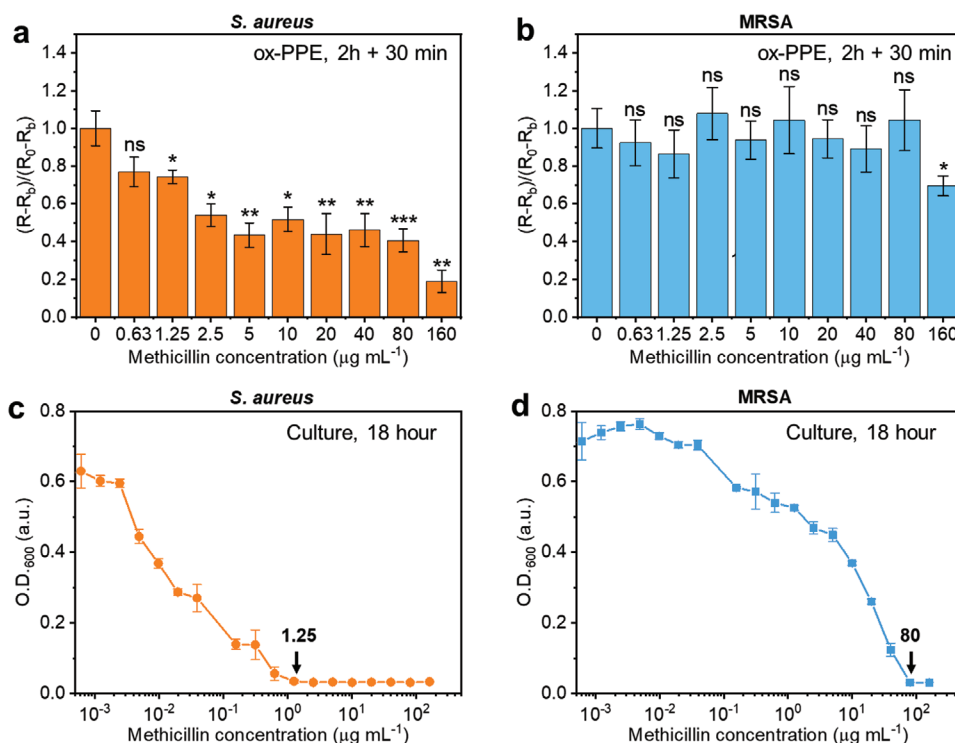

Figure 5. Susceptibility of *S. aureus* ATCC 6538 and MRSA USA300 toward methicillin (5 × 10^7 cells mL^{-1} in MHB medium), determined by a,b) relative reduction of ox-PPE or c,d) optical density of bacteria suspensions at 600 nm. Error bars represent standard deviation of triplicate measurements. ns: no significant difference; *$p < 0.05$; **$p < 0.01$; ***$p < 0.001$ in two-sample *t*-test with unequal variance. Absorption spectra were recorded after 2 h antibiotic exposure and 30 min ox-PPE reduction reaction. Optical densities were recorded after 18 h incubation.
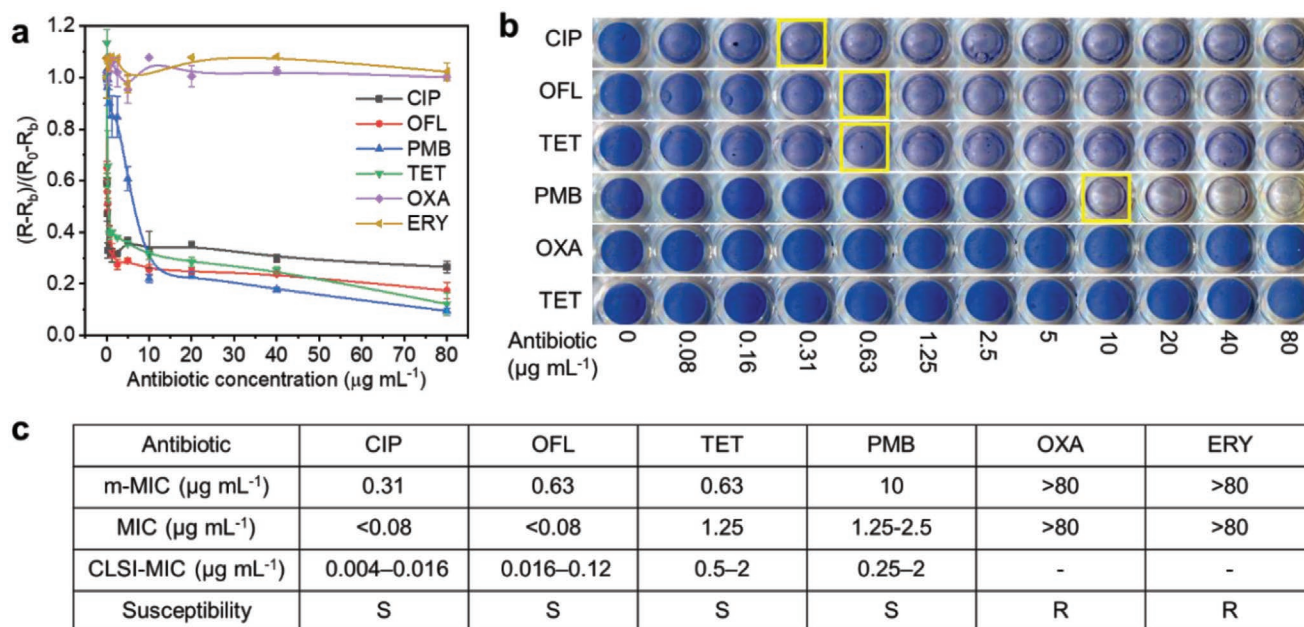
Figure 6. Evaluation of antimicrobial susceptibility of *E. coli* toward different antibiotics. a) Relative reduction of ox-PPE in *E. coli* suspensions (5×10^7 cells mL^{-1} in M9 medium containing 0.4% glucose). b) Photographic images of microplate wells showing the color change upon addition of varied antibiotics at different concentrations. c) Results of susceptibility of *E. coli* toward various antibiotics. m-MIC: the minimum concentration of antibiotic for metabolic reduction of ox-PPE to the bottom plateau. MIC: the minimum concentration of antibiotic to inhibit visual growth of bacteria, measured by the optical density of bacteria suspensions after 18 h incubation. CLSI-MIC: the reported MIC values from CLSI handbook. S: susceptible; R: resistant. Error bars represent standard deviation of triplicate measurements. Absorption spectra were recorded after 2 h antibiotic exposure and 1 h reaction (3 h in total).

into the suspensions and incubated for another 1 h before the photographs and the absorption spectra were recorded. The relative reduction degrees were plotted against the concentration of antibiotics (**Figure 6**a). To quantify the susceptibility, we defined a metabolic-minimum inhibitory concentration (m-MIC) that describes the minimum concentration of antibiotic for reduction of ox-PPE to reach the bottom plateau. Meanwhile, it is important to note that the m-MICs could also be estimated by naked eyes through the visual color change of ox-PPE (Figure 6b). The obtained m-MIC values were compared with the MIC determined by the conventional culture-based method (Figure S5, Supporting Information) as well as the MIC reported by Clinical & Laboratory Standards Institute (CLSI) handbook (CLSI-MIC) (Figure 6c). The antimicrobial susceptibility determined by our method is in good agreement with that by the conventional MIC and the reported CLSI-MIC. Nevertheless, we notice that the values of m-MIC are slightly larger than the other two in some cases. This is probably because the bacteria concentration we used ($\approx 5 \times 10^7$ cells mL^{-1}) was higher than the one used in the conventional tests ($\approx 5 \times 10^5$ cells mL^{-1}), and also the detection mechanisms are different. Collectively, ox-PPE allows facile evaluation of antimicrobial susceptibility toward different antibiotics in a rapid and high-throughput manner.

2.6. Discussion

Infectious diseases, especially bacterial infections, are emerging at an unprecedented rate, posing a grave challenge to public health and global economy.[27] Rapid discrimination of pathogens[28] and characterization of antimicrobial susceptibility[29] are the two key tasks to tackle this impending crisis.[30] Yet, conventional techniques for pathogen discrimination and antimicrobial susceptibility testing are laborious and time-consuming, resulting in the delay of patient treatment and high risk of severe infection.[18b,28b,31] Although polymerase chain reaction (PCR) and mass spectroscopy (MS) methods can achieve specific profiling and reduce the detection time to a few hours, they require large databases and lack the ability to directly test live bacteria's function.[31a,32] Therefore, there is an unmet need to develop simple, rapid, sensitive, and inexpensive tools for bacterial detection and discrimination, as well as susceptibility testing.

In recent years, molecular sensors have been developed for sensing of microbials, through colorimetric, photoluminescent, electrochemical, plasmon resonant, and other mechanisms.[33] Many of those microbial sensors are based on antibody-antigen recognitions or other specific ligand-receptor interactions,[34] whose usage is limited to only certain circumstances and cannot be applied to unknown pathogens. Thus, a more general and facile strategy is desired for bacterial discrimination. Taking advantages of the surface charge density, hydrophobicity and geometry of bacterial membranes, cationic oligomers,[35] cationic polymers,[36] cationic polymer complexes,[15a,16,37] and cationic aggregation-induced emission luminogens [15b] have been used for bacterial detection and discrimination by monitoring their fluorescence changes. However, such detection strategy is unable to differentiate live and dead bacteria,

and some of these materials suffer from high toxicity toward mammalian cells.[38] Polydiacetylene-assembled vesicles have also been used as colorimetric sensors, whose conformation changes upon interaction with molecules released by bacteria, leading to a visible blue to red color shift.[39] Yet, the sensitivity of solution-based polydiacetylene sensors often remains unsatisfactory.[40] More recently, metabolic sensing of bacteria through a click reaction has been demonstrated,[38a,41] but such covalent binding raises concerns in perturbing bacterial structure and functions in living settings.[42]

In this study, we introduced a water-soluble electrochromic ox-PPE, which undergoes extracellular reduction by the metabolites released by live bacteria. Our method avoids the perturbation of bacterial membrane. The reduction reaction is manifested with colorimetric and absorption spectroscopic changes, enabling facile detection without using any sophisticated instruments. In addition, the reaction shows generalities with different bacterial strains, and the ability to discriminate Gram-negative and Gram-positive bacteria. Compared to the classical gram staining method which involves multiple steps and prone to operator error,[31b] our method has superiority in its simplicity and cost effectiveness. Moreover, the synthesis of ox-PPE is much more cost-effective compared to nanoparticles or other complex materials. Last but not the least, our study extends the scope and versatility of electrochromic conjugated polymers.

Though we focused on bacterial detection and susceptibility testing here, applications of PPE can be extended to study of slow-growing organisms and to drug development. Our metabolism-based method is also promising to study slow-growing bacteria, because they do not grow normally to form colony but still have their metabolic activity.[43] On the other hand, since our detection mechanism is different from the conventional approaches, it is beneficial for developing new drugs with brand-new antimicrobial mechanisms. Furthermore, in the view of the potential imaging capabilities of this conjugated polymer,[44] it also holds great promise for in vivo imaging and diagnosis of infectious disease.[45]

Finally, we recognize that the current colorimetric change is relatively subtle for low concentrations of bacteria (Figure 2c; Figure S2, Supporting Information). Further molecular engineering can be carried out to improve the sensitivity, such as tuning the lowest unoccupied molecular orbital and the highest occupied molecular orbital of the conjugated polymers.[14a] Another potential approach to amplify the signal readout is to make organic electrochemical transistor, which can provide amplified electric signals and be combined with colorimetric detection.[46] Meanwhile, we also recognize that the role of transmembrane electron transfer in the reduction of ox-PPE can be defined in the future study.

3. Conclusion

Water-soluble electrochromic ox-PPE was introduced for bacterial detection, discrimination, and susceptibility testing in a rapid, facile, and high-throughput format. Reducing metabolites released by active bacteria were shown to be the underlying mechanism for the reduction of ox-PPE. We demonstrated the capability of ox-PPE for differentiation of Gram-negative and Gram-positive

bacteria, distinguishing between resistant and susceptible bacterial strains, as well as evaluation of antimicrobial susceptibility to different antibiotics. This simple, cost-effective, high-throughput, and rapid method opens exciting opportunities toward personalized diagnosis and prescription of infectious diseases.

4. Experimental Section

Polymer Synthesis: PPE was synthesized as reported previously.[14b] Briefly, an organic-soluble polymer was synthesized by direct (hetero) arylation polymerization of 3,4-ethylenedioxythiophene (EDOT) with a 3,4-propylenedioxythiophene (ProDOT) derivative bearing esterfunctionalized side chains. Then, the ester side chains were hydrolyzed by 2 M KOH to water-soluble carboxylate salts.

Preparation of ox-PPE: PPE was first dissolved in 0.1 M NaOH aqueous solution. Then, the solution pH was tuned to 7.4 by adding HCl. 1 mg mL^{-1} ox-PPE was prepared as stock solutions.

Preparation of E. coli Suspensions in M9 Medium: Two colonies of bacteria on tryptic soy agar plates were transferred to 4 mL of liquid TSB culture medium and grown at 37 °C for 4 h. Bacteria were harvested by centrifuging at 3000 rpm for 3 min. After removal of supernatant, fresh M9 medium containing 0.4% glucose was added to resuspend bacteria. The concentrations of bacteria were determined by measuring optical density at 600 nm (O.D.$_{600}$) and then diluted into desired concentration (e.g., O.D.$_{600}$ 0.5 = 10^8 cells mL^{-1}). Bacteria were allocated to 96-well microplates with 100 µL per well and kept at 37 °C (or 4 °C) for 2 h. Then, 100 µL ox-PPE (50 µg mL^{-1}) was added to each well, resulting a final concentration of 25 µg mL^{-1} ox-PPE.

Preparation of Suspensions of Different Bacterial Strains in MHB Medium: Colonies of bacteria on tryptic soy agar plates were transferred to 4 mL of liquid MHB culture medium and grown at 37 °C for 4 h at a shaking speed of 200 rpm. The bacterial concentrations were determined by measuring optical density at 600 nm (O.D.$_{600}$) and then diluted into desired concentration (0.5 O.D.$_{600}$ = 10^8 cells mL^{-1}). 100 µL bacteria and 100 µL ox-PPE (50 µg mL^{-1}) was added to each well in sequence, resulting a final concentration of 25 µg mL^{-1} ox-PPE.

Susceptibility Measurements: Bacteria were cultured and diluted as previously mentioned. 5 × 10^7 cells mL^{-1} bacteria (O.D.$_{600}$ = 0.25) were allocated to 96-well microplates (100 µL per well) and exposed to antibiotics for 2 h at 37 °C. Then, 100 µL ox-PPE (50 µg mL^{-1}) was added to each well, resulting a final concentration of 25 µg mL^{-1} ox-PPE. After adding ox-PPE, the plates were kept at 37 °C for another 30 min or 1 h.

Optical Absorption Spectroscopy Measurements and Photographic Images: Optical measurements were carried out with a SpectraMax i3x Multi-Mode microplate reader. The images were recorded by EPSON V370 photoscanner.

Transient-Absorption Imaging: An 80 MHz repetition rate femtosecond pulsed laser (Spectra Physics, InSight X3) provided two synchronized outputs: a fixed 1045 nm beam with ≈200 fs pulse width and a tunable beam ranging from 680 to 1300 nm with ≈120 fs pulse width. In the TA microscopy system, the fixed 1045 nm beam served as pump source and the other beam served as probe beam was tuned to 853 nm. The resulted laser beating frequency (2154 cm^{-1}) was at Raman silent region, avoiding any signals from the biological systems. The pump beam was modulated at 2.3 MHz by an acousto-optic modulator (Isomet, 1205-C). Temporal delay between the pump and probe pulses was controlled by a motorized translation stage (Zaber, TLS28E), and collinearly combined and directed into a homebuilt laser-scanning microscope. Then, the pump and probe beams were focused on the sample by a 60× water immersion objective (NA = 1.2, UPlanApo/IR, Olympus), and the forward signals were collected by an oil condenser (NA = 1.4, U-AAC, Olympus). After passing an 850 ± 120 nm bandpass filter, the 1045 nm light was blocked and the TA signals (change in the intensity of 853 nm probe beam) were detected by a photodiode (Hamamatsu, S3994) incorporated with a home-built resonant circuit, and then demodulated by a phase-sensitive lock-in amplifier (Zurich Instruments). All images were acquired with

10 µs pixel^{-1} dwell time. The probe (853 nm) and pump (1045 nm) powers before the microscope were maintained at 5 and 5 mW, respectively.

Culture-Based MIC Measurements: Bacteria ($\approx 5 \times 10^5$ cells mL^{-1}) suspensions containing different concentrations of antibiotics were incubated at 37 °C for 18 h and then the optical density at 600 nm was recorded, and culture-based MIC was determined as the lowest concentration, which inhibits the visible growth of bacteria.

Potentiometric UV–Vis Titration Curve Fitting: Potentiometric UV–vis titration curve fitting[24] was performed to extract the UV–vis absorption spectrum of neutral state, polaron, and bipolaron PPE, respectively. First, the electrode potentials in the potentiometric titration was converted to the concentration of a hypothetical redox pair ([G] and [G$^+$]) by applying Nernst equation

$$E = E^\theta - \frac{RT}{F}\ln\frac{[G]}{[G^+]} \tag{2}$$

Here, E is the electrode potential in the potentiometric titration, R is ideal gas constant, T is the temperature of the titration, F is Faraday's constant, and E^θ is the standard electrode potential of the hypothetical redox pair and it is set to 0 for convenient calculation. Then, the fitting was established based on chemical equilibrium model

$$\Delta A = \frac{(\varepsilon_P - \varepsilon_{BP})[H]_0 K_1 \frac{[G]}{[G^+]} (\varepsilon_N - \varepsilon_{BP})[H]_0 K_1 K_2 \left(\frac{[G]}{[G^+]}\right)^2}{1 + K_1 \frac{[G]}{[G^+]} + K_1 K_2 \left(\frac{[G]}{[G^+]}\right)^2} \tag{3}$$

Here, ε_{BP}, ε_P, and ε_N are the molar extinction coefficients of bipolaron, polaron, and neutral state, respectively. $[H]_0$ is the initial concentration of the polymer, K_1 and K_2 are the equilibrium constants of the hypothetical redox reaction. The fitting was performed on BindFit, an open source online software (http://supramolecular.org). Notably, among the output parameters, only the molar extinction coefficients were meaningful, while the equilibrium constants were meaningless due to the nature of the input.

Supporting Information

Supporting Information is available from the Wiley Online Library or from the author.

Acknowledgements

Conflict of Interest

The authors declare no conflict of interest.

Keywords

[1] a) J. L. Bredas, G. B. Street, *Acc. Chem. Res.* **1985**, *18*, 309; b) J. R. Platt, *J. Chem. Phys.* **1961**, *34*, 862; c) P. M. Monk, R. J. Mortimer, D. R. Rosseinsky, *Electrochromism: Fundamentals and Applications*, John Wiley & Sons, New York **2008**.

[2] a) H. Yu, S. Shao, L. Yan, H. Meng, Y. He, C. Yao, P. Xu, X. Zhang, W. Hu, W. Huang, *J. Mater. Chem. C* **2016**, *4*, 2269; b) G. Cai, J. Wang, P. S. Lee, *Acc. Chem. Res.* **2016**, *49*, 1469; . c) R. J. Mortimer, A. L. Dyer, J. R. Reynolds, *Displays* **2006**, *27*, 2; d) A. L. Dyer, R. H. Bulloch, Y. Zhou, B. Kippelen, J. R. Reynolds, F. Zhang, *Adv. Mater.* **2014**, *26*, 4895; . e) A. M. Österholm, D. E. Shen, J. A. Kerszulis, R. H. Bulloch, M. Kuepfert, A. L. Dyer, J. R. Reynolds, *ACS Appl. Mater. Interfaces* **2015**, *7*, 1413; f) M. A. Invernale, Y. Ding, G. A. Sotzing, *ACS Appl. Mater. Interfaces* **2010**, *2*, 296.

[3] a) S. A. Sapp, G. A. Sotzing, J. R. Reynolds, *Chem. Mater.* **1998**, *10*, 2101; b) L. Groenendaal, G. Zotti, P. H. Aubert, S. M. Waybright, J. R. Reynolds, *Adv. Mater.* **2003**, *15*, 855; c) G. Sonmez, H. B. Sonmez, C. K. Shen, R. W. Jost, Y. Rubin, F. Wudl, *Macromolecules* **2005**, *38*, 669; d) J. A. Kerszulis, C. M. Amb, A. L. Dyer, J. R. Reynolds, *Macromolecules* **2014**, *47*, 5462; e) J. Padilla, A. M. Österholm, A. L. Dyer, J. R. Reynolds, *Sol. Energy Mater. Sol. Cells* **2015**, *140*, 54; f) A. A. Argun, P.-H. Aubert, B. C. Thompson, I. Schwendeman, C. L. Gaupp, J. Hwang, N. J. Pinto, D. B. Tanner, A. G. MacDiarmid, J. R. Reynolds, *Chem. Mater.* **2004**, *16*, 4401.

[4] N. Casado, G. Hernández, H. Sardon, D. Mecerreyes, *Prog. Polym. Sci.* **2016**, *52*, 107.

[5] a) D. T. Simon, E. O. Gabrielsson, K. Tybrandt, M. Berggren, *Chem. Rev.* **2016**, *116*, 13009; . b) E. Cabane, X. Zhang, K. Langowska, C. G. Palivan, W. Meier, *Biointerphases* **2012**, *7*, 9; c) N. Aydemir, J. Malmstrom, J. Travas-Sejdic, *Phys. Chem. Chem. Phys.* **2016**, *18*, 8264.

[6] a) V. S. A. Piriya, P. Joseph, S. C. G. K. Daniel, S. Lakshmanan, T. Kinoshita, S. Muthusamy, *Mater. Sci. Eng., C* **2017**, *78*, 1231; b) Z. Li, J. R. Askim, K. S. Suslick, *Chem. Rev.* **2019**, *119*, 231; c) M. A. Deshmukh, M. Gicevicius, A. Ramanaviciene, M. D. Shirsat, R. Viter, A. Ramanavicius, *Sens. Actuators, B* **2017**, *248*, 527; d) B. Kondratowicz, R. Narayanaswamy, K. C. Persaud, *Sens. Actuators, B* **2001**, *74*, 138.

[7] B. Thakur, C. A. Amarnath, S. H. Mangoli, S. N. Sawant, *Sens. Actuators, B* **2015**, *207*, 262.

[8] a) F. Kracke, I. Vassilev, J. O. Kromer, *Front. Microbiol.* **2015**, *6*, 575; b) S. H. Light, L. Su, R. Rivera-Lugo, J. A. Cornejo, A. Louie, A. T. Iavarone, C. M. Ajo-Franklin, D. A. Portnoy, *Nature* **2018**, *562*, 140; c) M. V. Berridge, P. M. Herst, A. S. Tan, *Biotechnol. Annu. Rev.* **2005**, *11*, 127.

[9] a) Z.-C. Yang, Y.-Y. Cheng, F. Zhang, B.-B. Li, Y. Mu, W.-W. Li, H.-Q. Yu, *Environ. Sci. Technol. Lett.* **2016**, *3*, 133; b) S. J. Yuan, W. W. Li, Y. Y. Cheng, H. He, J. J. Chen, Z. H. Tong, Z. Q. Lin, F. Zhang, G. P. Sheng, H. Q. Yu, *Nat. Protoc.* **2014**, *9*, 112.

[10] a) G. Rodriguez, D. Phipps, K. Ishiguro, H. Ridgway, *Appl. Environ. Microbiol.* **1992**, *58*, 1801; b) M. V. Berridge, A. S. Tan, *Protoplasma* **1998**, *205*, 74; c) J.-S. Chang, B.-Y. Chen, Y. S. Lin, *Bioresour. Technol.* **2004**, *91*, 243; d) J. C. Palomino, A. Martin, M. Camacho, H. Guerra, J. Swings, F. Portaels, *Antimicrob. Agents Chemother.* **2002**, *46*, 2720.

[11] V. Créach, A.-C. Baudoux, G. Bertru, B. L. Rouzic, *J. Microbiol. Methods* **2003**, *52*, 19.

[12] S. Ullrich, B. Karrasch, H. Hoppe, K. Jeskulke, M. Mehrens, *Appl. Environ. Microbiol.* **1996**, *62*, 4587.

[13] a) G. Smirnova, N. Muzyka, O. Oktyabrsky, *Microbiol. Res.* **2012**, *167*, 166; b) H. Takagi, I. Ohtsu, in *Amino Acid Fermentation* (Eds: A. Yokota, M. Ikeda), Springer Japan, Tokyo **2017**, pp. 129–151; c) T. Oguri, B. Schneider, L. Reitzer, *J. Bacteriol.* **2012**, *194*, 4366.

[14] a) J. F. Ponder Jr, A. M. Österholm, J. R. Reynolds, *Macromolecules* **2016**, *49*, 2106; b) J. F. Ponder Jr, A. M. Österholm, J. R. Reynolds, *Chem. Mater.* **2017**, *29*, 4385.

[15] a) C. Zhu, Q. Yang, L. Liu, S. Wang, *Angew. Chem.* **2011**, *50*, 9607; b) E. Zhao, Y. Chen, S. Chen, H. Deng, C. Gui, C. W. Leung, Y. Hong, J. W. Lam, B. Z. Tang, *Adv. Mater.* **2015**, *27*, 4931.

[16] O. R. Miranda, X. Li, L. Garcia-Gonzalez, Z. J. Zhu, B. Yan, U. H. Bunz, V. M. Rotello, *J. Am. Chem. Soc.* **2011**, *133*, 9650.

**ADVANCED
SCIENCE NEWS**

www.advancedsciencenews.com

**ADVANCED
FUNCTIONAL
MATERIALS**

www.afm-journal.de

[17] N. Bhardwaj, S. K. Bhardwaj, D. Bhatt, D. K. Lim, K.-H. Kim, A. Deep, *TrAC, Trends Anal. Chem.* **2019**, *113*, 280.

[18] a) T. E. Shehata, A. G. Marr, *J. Bacteriol.* **1971**, *107*, 210; b) G. Longo, L. Alonso-Sarduy, L. M. Rio, A. Bizzini, A. Trampuz, J. Notz, G. Dietler, S. Kasas, *Nat. Nanotechnol.* **2013**, *8*, 522.

[19] S. A. Hice, M. C. Santoscoy, M. L. Soupir, R. Cademartiri, *Appl. Microbiol. Biotechnol.* **2018**, *102*, 367.

[20] J. Wu, H. J. Lee, L. You, X. Luo, T. Hasegawa, K. C. Huang, P. Lin, T. Ratliff, M. Ashizawa, J. Mei, *Small* **2020**, *16*, 2001215.

[21] D. Denk, A. Böck, *Microbiology* **1987**, *133*, 515.

[22] R. A. Owens, P. E. Hartman, *J. Bacteriol.* **1986**, *168*, 109.

[23] a) S. Wold, K. Esbensen, P. Geladi, *Chemom. Intell. Lab. Syst.* **1987**, *2*, 37; b) J. Shen, R. Hu, T. Zhou, Z. Wang, Y. Zhang, S. Li, C. Gui, M. Jiang, A. Qin, B. Z. Tang, *ACS Sens.* **2018**, *3*, 2218.

[24] a) P. Thordarson, *Chem. Soc. Rev.* **2011**, *40*, 1305; b) D. Brynn Hibbert, P. Thordarson, *Chem. Commun.* **2016**, *52*, 12792.

[25] a) M. Imber, A. J. Pietrzyk-Brzezinska, H. Antelmann, *Redox Biol.* **2019**, *20*, 130; b) V. V. Loi, M. Rossius, H. Antelmann, *Front. Microbiol.* **2015**, *6*, 187.

[26] N. Kaldalu, R. Mei, K. Lewis, *Antimicrob. Agents Chemother.* **2004**, *48*, 890.

[27] a) World Health Organization, *Antimicrobial Resistance: Global Report on Surveillance*, World Health Organization, Geneva, Switzerland **2014**; b) U.S. Department of Health and Human Services, *Antibiotic Resistance Threats in the United States*, US Department of Health and Human Services, CDC, Atlanta, GA **2013**; c) K. E. Jones, N. G. Patel, M. A. Levy, A. Storeygard, D. Balk, J. L. Gittleman, P. Daszak, *Nature* **2008**, *451*, 990.

[28] a) A. Sharma, N. Sharma, A. Kumari, H.-J. Lee, T. Kim, K. M. Tripathi, *Appl. Mater. Today* **2020**, *18*, 100467; b) G. Maugeri, I. Lychko, R. Sobral, A. C. A. Roque, *Biotechnol. J.* **2019**, *14*, 1700750.

[29] L. B. Reller, M. Weinstein, J. H. Jorgensen, M. J. Ferraro, *Clin. Infect. Dis.* **2009**, *49*, 1749.

[30] H. Leonard, R. Colodner, S. Halachmi, E. Segal, *ACS Sens.* **2018**, *3*, 2202.

[31] a) Y. Tang, L. Zhen, J. Liu, J. Wu, *Anal. Chem.* **2013**, *85*, 2787; b) T. J. Beveridge, *Biotech. Histochem.* **2001**, *76*, 111.

[32] W. Florio, A. Tavanti, S. Barnini, E. Ghelardi, A. Lupetti, *Front. Microbiol.* **2018**, *9*, 1097.

[33] C. E. Rowland, C. W. Brown, J. B. Delehanty, I. L. Medintz, *Mater. Today* **2016**, *19*, 464.

[34] a) N. Mohanty, V. Berry, *Nano Lett.* **2008**, *8*, 4469; b) Y. Huang, X. Dong, Y. Liu, L.-J. Li, P. Chen, *J. Mater. Chem.* **2011**, *21*, 12358; c) H. M. So, D. W. Park, E. K. Jeon, Y. H. Kim, B. S. Kim, C. K. Lee, S. Y. Choi, S. C. Kim, H. Chang, J. O. Lee, *Small* **2008**, *4*, 197; d) R. A. Villamizar, A. Maroto, F. X. Rius, I. Inza, M. J. Figueras, *Biosens. Bioelectron.* **2008**, *24*, 279; e) Z. Z. Chen, L. Cai, M. Y. Chen, Y. Lin, D. W. Pang, H. W. Tang, *Biosens. Bioelectron.* **2015**, *66*, 95; f) L. C. Ong, L. Y. Ang, S. Alonso, Y. Zhang, *Biomaterials* **2014**, *35*, 2987; g) S. Wu, N. Duan, Z. Shi, C. Fang, Z. Wang, *Anal. Chem.* **2014**, *86*, 3100; h) H. Xin, Y. Li, D. Xu, Y. Zhang, C. H. Chen, B. Li, *Small* **2017**, *13*, 1603418; i) L. Yang, Y. Li, *Analyst* **2006**, *131*, 394.

[35] a) A. W. Thomas, C. Catania, L. E. Garner, G. C. Bazan, *Chem. Commun.* **2015**, *51*, 9294; b) B. Wang, M. Wang, A. Mikhailovsky, S. Wang, G. C. Bazan, *Angew. Chem.* **2017**, *56*, 5031.

[36] a) H. Yuan, Z. Liu, L. Liu, F. Lv, Y. Wang, S. Wang, *Adv. Mater.* **2014**, *26*, 4333; b) S. Zhu, X. Wang, Y. Yang, H. Bai, Q. Cui, H. Sun, L. Li, S. Wang, *Chem. Mater.* **2018**, *30*, 3244.

[37] a) H. Bai, H. Chen, R. Hu, M. Li, F. Lv, L. Liu, S. Wang, *ACS Appl. Mater. Interfaces* **2016**, *8*, 31550; b) H. Bai, H. Zhang, R. Hu, H. Chen, F. Lv, L. Liu, S. Wang, *Langmuir* **2017**, *33*, 1116; c) H. Yuan, H. Zhao, K. Peng, R. Qi, H. Bai, P. Zhang, Y. Huang, F. Lv, L. Liu, J. Bao, S. Wang, *ACS Appl. Mater. Interfaces* **2020**, *12*, 21263; d) R. L. Phillips, O. R. Miranda, C. C. You, V. M. Rotello, U. H. Bunz, *Angew. Chem.* **2008**, *47*, 2590; e) C. Zhu, Q. Yang, L. Liu, S. Wang, *J. Mater. Chem.* **2011**, *21*, 7905.

[38] a) M. Wu, G. Qi, X. Liu, Y. Duan, J. Liu, B. Liu, *Chem. Mater.* **2020**, *32*, 858; b) D. Fischer, Y. Li, B. Ahlemeyer, J. Krieglstein, T. Kissel, *Biomaterials* **2003**, *24*, 1121; c) O. Lunov, T. Syrovets, C. Loos, J. Beil, M. Delacher, K. Tron, G. U. Nienhaus, A. Musyanovych, V. Mailander, K. Landfester, *ACS Nano* **2011**, *5*, 1657.

[39] a) J. Park, S. K. Ku, D. Seo, K. Hur, H. Jeon, D. Shvartsman, H. K. Seok, D. J. Mooney, K. Lee, *Chem. Commun.* **2016**, *52*, 10346; b) L. Silbert, I. Ben Shlush, E. Israel, A. Porgador, S. Kolusheva, R. Jelinek, *Appl. Environ. Microbiol.* **2006**, *72*, 7339.

[40] X. Qian, B. Städler, *Chem. Mater.* **2019**, *31*, 1196.

[41] a) P. Shieh, M. S. Siegrist, A. J. Cullen, C. R. Bertozzi, *Proc. Natl. Acad. Sci. USA* **2014**, *111*, 5456; b) H. Liang, K. E. DeMeester, C. W. Hou, M. A. Parent, J. L. Caplan, C. L. Grimes, *Nat. Commun.* **2017**, *8*, 15015; c) D. Mao, F. Hu, S. J. i. Kenry, W. Wu, D. Ding, D. Kong, B. Liu, *Adv. Mater.* **2018**, *30*, 1706831.

[42] H. L. Chan, L. Lyu, J. Aw, W. Zhang, J. Li, H. H. Yang, H. Hayashi, S. Chiba, B. Xing, *ACS Chem. Biol.* **2018**, *13*, 1890.

[43] K. Dong, H. Pan, D. Yang, L. Rao, L. Zhao, Y. Wang, X. Liao, *Compr. Rev. Food Sci. Food Saf.* **2020**, *19*, 149.

[44] a) Q. Miao, C. Xie, X. Zhen, Y. Lyu, H. Duan, X. Liu, J. V. Jokerst, K. Pu, *Nat. Biotechnol.* **2017**, *35*, 1102; b) Y. Lyu, D. Cui, J. Huang, W. Fan, Y. Miao, K. Pu, *Angew. Chem.* **2019**, *131*, 5037; c) J. Huang, C. Xie, X. Zhang, Y. Jiang, J. Li, Q. Fan, K. Pu, *Angew. Chem., Int. Ed.* **2019**, *58*, 15120; d) D. Cui, P. Li, X. Zhen, J. Li, Y. Jiang, A. Yu, X. Hu, K. Pu, *Adv. Funct. Mater.* **2019**, *29*, 1903461.

[45] Z. Mei, D. Gao, D. Hu, H. Zhou, T. Ma, L. Huang, X. Liu, R. Zheng, H. Zheng, P. Zhao, *Biomaterials* **2020**, *251*, 120092.

[46] J. Rivnay, S. Inal, A. Salleo, R. M. Owens, M. Berggren, G. G. Malliaras, *Nat. Rev. Mater.* **2018**, *3*, 17086.

2005192 (10 of 10)